Supporting Information

Impact of rotational twin boundaries and lattice mismatch on III-V nanowire growth

Matthias Steidl[1]*, Christian Koppka[1‡], Lars Winterfeld[2‡], Katharina Peh[1], Beatriz Galiana Blanco[3], Oliver Supplie[1], Peter Kleinschmidt[1], Erich Runge[2], Thomas Hannappel[1]*

[1] Department of Photovoltaics, Institute of Physics and Institute of Micro- and Nanotechnologies, TU Ilmenau, 98693 Ilmenau, Germany

[2] Department of Theoretical Physics I, Institute of Physics and Institute of Micro- and Nanotechnologies, TU Ilmenau, 98693 Ilmenau, Germany

[3] Physics Department, Universidad Carlos III de Madrid, 28911 Madrid, Spain

*To whom correspondence should be addressed: thomas.hannappel@tu-ilmenau.de, matthias.steidl@tu-ilmenau.de

‡These authors contributed equally.

S1 Nanowire growth on reference samples

This section presents some SEM images of nanowires grown on reference substrates, which are referred to in the main text. This includes GaP nanowire growth both on GaP(111)B and GaP(111)A, shown in Figure S1a and b, respectively. Moreover, GaAs nanowires grown on GaP(111)B with different growth durations and view angles are presented in Figure S2.

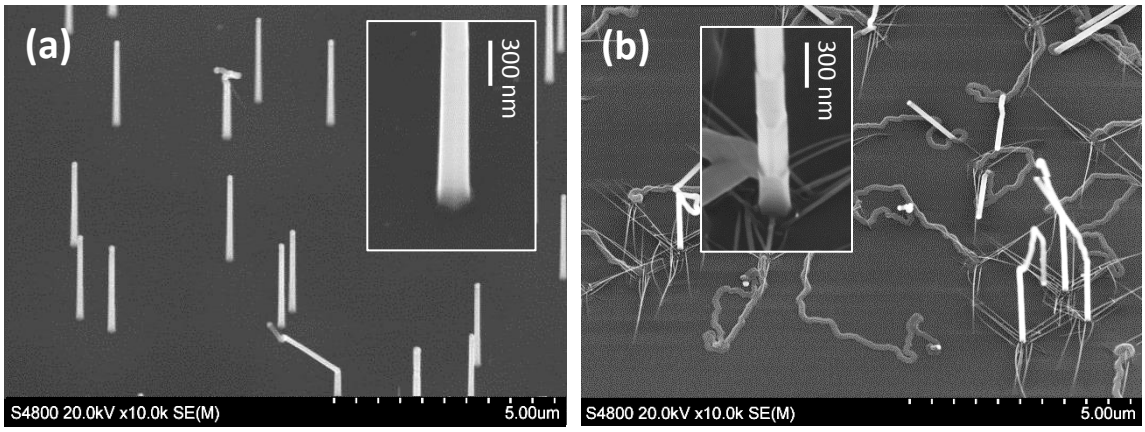

Figure S1: GaP nanowires on a GaP(111)B wafer piece (a) and on a GaP(111)A wafer piece (b).

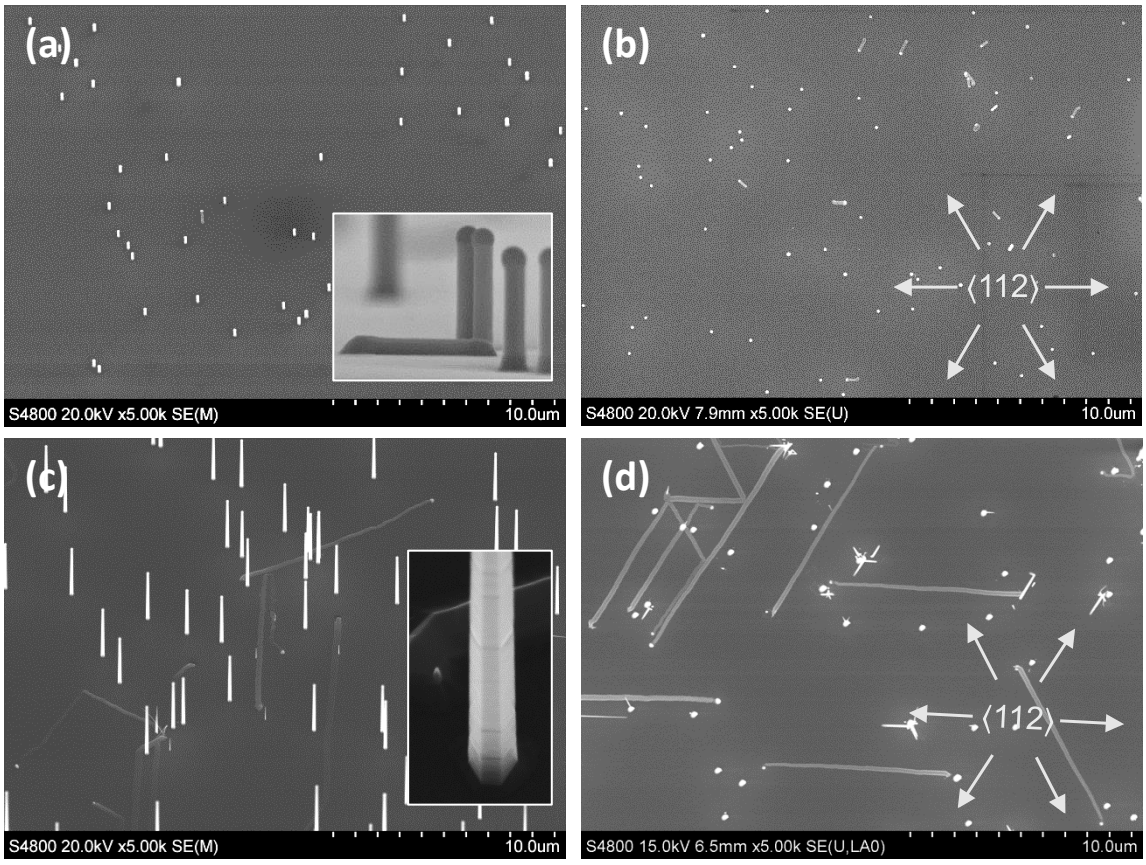

Figure S2: GaAs nanowires (NWs) on GaP(111)B wafer pieces with different growth durations: (a) and (b) 1 minute, (c) and (d) 12 minutes. While panels (a) and (c) display a tilt view of a representative spot on the respective sample, panels (b) and (d) show numerous horizontal NWs growing in ⟨112⟩ direction from the top. Note that the vertical NW shown in the inset of (c) exhibits numerous grooves at the side facets, which are reflecting stacking faults within the NW.

S2 Diagonal GaP nanowires

This section gives additional information about diagonal nanowires. It compares the observed growth directions with ones theoretically predicted by multiple order twinning at {111} facets.

Figure S3: Angle pairs for 75 different diagonal GaP nanowires. The angles α and φ are defined according to Uccelli et al.[1] and illustrated in Figure S4. The colored areas illustrate the relevant theoretically predicted growth directions that are possible by 3D (multiple order) twinning at {111} facets.

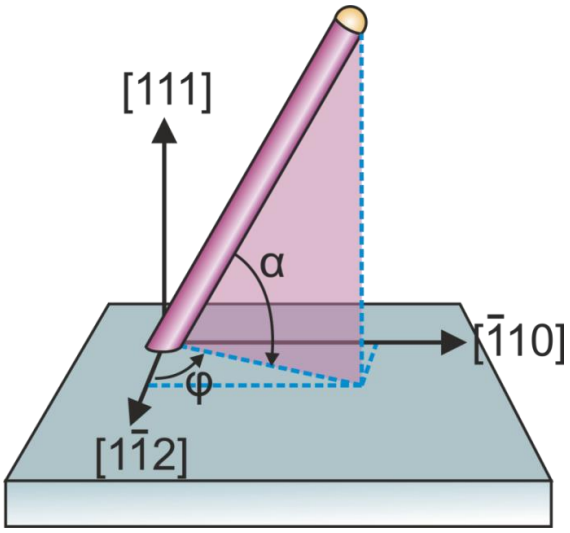

Figure S4: Definition of the angles α and φ according to Ref. 1.

S3 Different horizontal GaAs nanowires on GaP/Si(111)

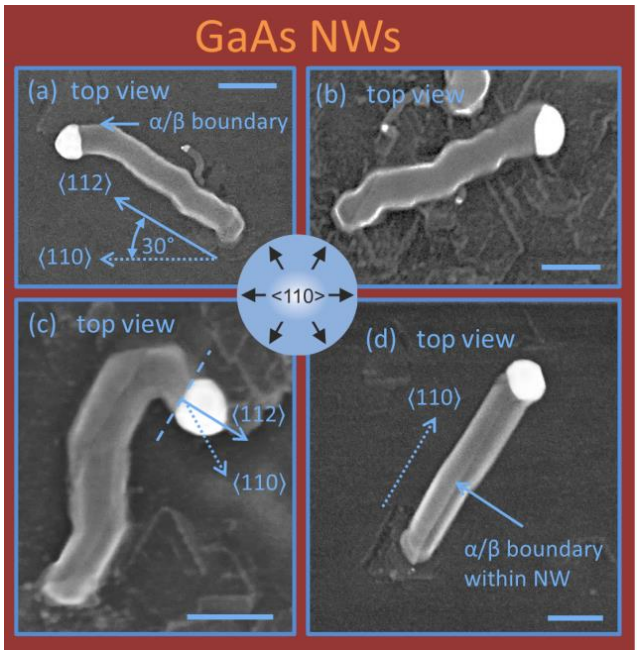

Figure S5: Various horizontal GaAs nanowires on GaP/Si(111). The scale bars are 200nm.

The growth of (heteroepitaxial) GaAs nanowires (NWs) exhibits a variety of different growth phenomena associated with rotational twin boundaries (RTBs). First of all, growth starting at RTBs always induces horizontal growth. Furthermore, RTBs trap gold particles and thereby cause growth along ⟨110⟩ directions instead of the common ⟨112⟩ directions (without RTB). This guiding behavior becomes apparent in the Figures S5a-c. The NW in Figure S5a first grows in a ⟨112⟩ direction and then continues growth in a ⟨110⟩ direction when it encounters the RTB. Similarly, the NWs shown in part b and c undergo several growth direction changes caused by the RTB-textured substrate surface. Note that in Figure S5c the growth direction and the growth interface point in two different azimuthal directions, ⟨112⟩ and ⟨110⟩, which are separated by 30°.

The NW in Figure S5d exhibits a peculiar morphology. It is streaked by a groove in ⟨110⟩ direction dividing it in two parts. In addition, its growth front comprises two facets pointing to each other. This strongly suggests that this NW itself contains an RTB, which most likely developed by simultaneous nucleation on the α and the β domain of the underlying substrate. Interestingly, this type of NW is the only one observed which preferably grows in ⟨110⟩ direction away from an RTB.

It is important to stress though that horizontal NW growth is not necessarily induced by RTBs. On the sample shown in Figure 2d for example, around 45% of the horizontal NWs can clearly be assigned to RTBs, 25 % initiate at undefined defects and for 30% no defect can be observed. Accordingly, growth on GaP(111)B (see Figure S2 and the statistics in Figure 2) yields around 5 % horizontal NWs. As discussed in literature,[2–6] the facet formation between Au and the underlying substrate prior to NW growth is crucial for the growth direction of a NW. When NW growth initiates, there is a dynamic interplay of facet growth and introduction of new facets,[6,7] which decides over the final growth direction. In case of heteroepitaxial NW growth,

we expect that the lattice strain strongly impedes the growth of the first few NW layers parallel to the substrate surface. This favors the formation of wedge-shaped structures, which require less strain energy, leading to the formation of a horizontal NW as depicted in Figure 5.

S4 No nanowire growth despite Au-particle: 'Au only'

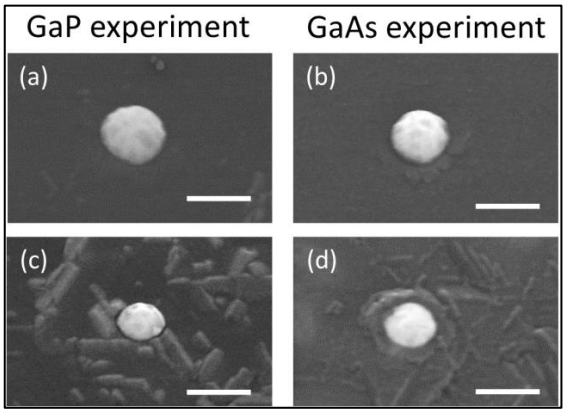

Figure S6: No nanowire growth despite Au-particle and appropriate precursor flow – (a) and (b) on GaP/Si(111) substrates with low twin density – (c) and (d) for high twin density. The scale bars are 200 nm.

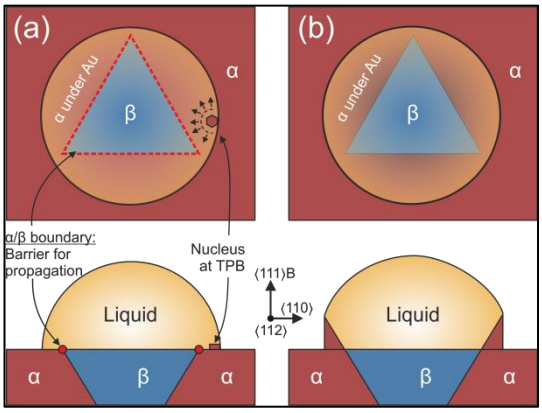

Figure S7: Mechanism for nanowire growth suppression. (a) Au-particle on top of a whole RTD (β) – (b) after growth of several annular layers

A frequent observation after nanowire (NW) growth experiments on GaP/Si(111) substrates is Au-particles without NW (referred to as *Au only*). For GaP and GaAs NW growth experiments the same tendency is observed: the lower the rotational twin density, the lower the ratio of Au-particles found without NW. In case of GaP(111)B wafer pieces as substrates, *i.e.* no rotational twins, Au-particles without NW are not found at all. Despite the clear dependence on the twin density, many of these Au-particles do not seem to be in the vicinity of rotational twin boundaries (RTBs), like the ones shown in Figure S6a and b. We assume that these Au particles are on top of a rotational twin domain (RTD) and cover its entire surface, preventing the direct observation of an RTD. Note that the RTDs can have diameters well below 100 nm.

A possible suppression mechanism is illustrated in Figure S7. Panel S7a shows a Au-particle covering a whole RTD before growth from the top and from the side. It is known that nucleation processes are limited to nucleation at the triple phase boundary (TPB) for most NW growth process conditions.[8,9] Once a stable nucleus forms at the TPB, it will expand until it reaches the RTB leading to an annular layer. Growth propagation across the RTB will strongly be impeded due to the energetically unfavorable positions for (single) atoms beyond this boundary. To enable growth on the β-domain, new nuclei would have to form far away from TPB – an unlikely process for these growth conditions. Instead, new nuclei will form at the TPB on top the former layer leading to annular layer-by-layer growth. This process will stop as soon as the Au-particle is either too distorted to wet the growth front or by a narrowing of the growth front (as depicted in Figure S7b).

S5 Growth facets of horizontal GaAs nanowires on GaP(111)B

The growth facet formation of a variety of horizontal GaAs NWs was investigated by SEM. Side views reveal that both {111}B and {111}A growth facets exist. This is evident, as for {111}B facets the normal vector points downwards to the substrate, whereas it points upwards for {111}A. In case of a strict epitaxial relation between NW and substrate, B-type NWs grow towards $\{\bar{1}\bar{1}2\}$, while A-type NWs grow in the opposite direction, towards $\{11\bar{2}\}$. Therefore, B-type NWs that grow towards $\{11\bar{2}\}$ can only be understood by a rotation of the crystal lattice of the NW by 180° around the [111] surface normal; likewise, A-type NWs towards $\{\bar{1}\bar{1}2\}$. The NWs in this so-called mirrored configuration are consequentially rotational twins. For statistical purpose, 32 NWs were closely examined like the ones presented in Figure S8. It was found that more than 87% of the NWs exhibit B-type facets and approx. 80% have the normal (untwinned) configuration.

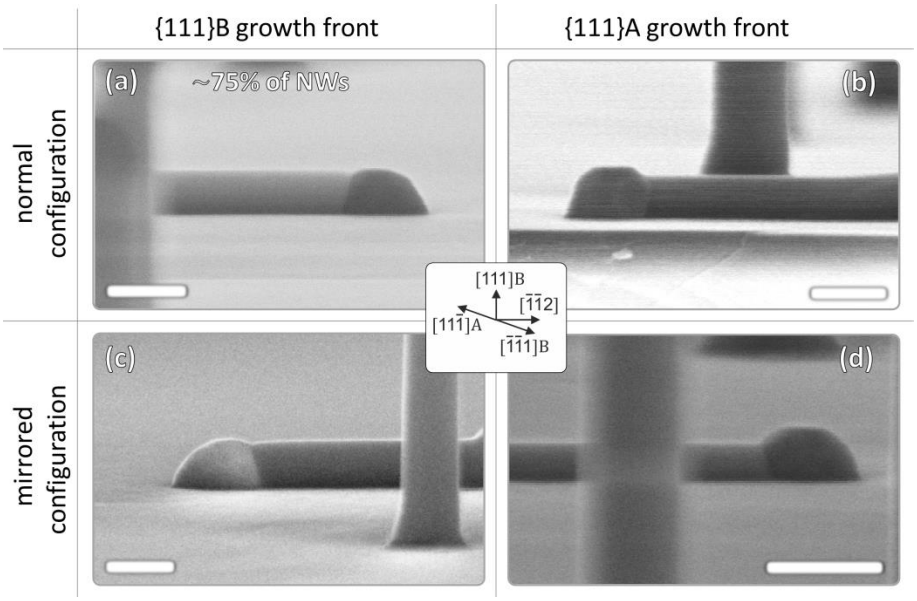

Figure S8: Side views on horizontal GaAs-NWs grown on GaP(111)B imaged by SEM. Normal and mirrored configuration differ in that the lattice of the NW in the mirrored configuration is rotated by 180° around the [111] surface normal. The vast majority of NWs (>87%) exhibit a {111}B facet, while for some NWs a {111}A facet is observed. The scale bars are 100 nm.

S6 TEM investigation of GaAs nanowires on GaP(111)B

Additional data on stacking faults in GaAs NWs, which grow in two different directions, is presented in this section. The data support the theoretical prediction of nucleation at quadruple phase boundaries for horizontal NW growth.

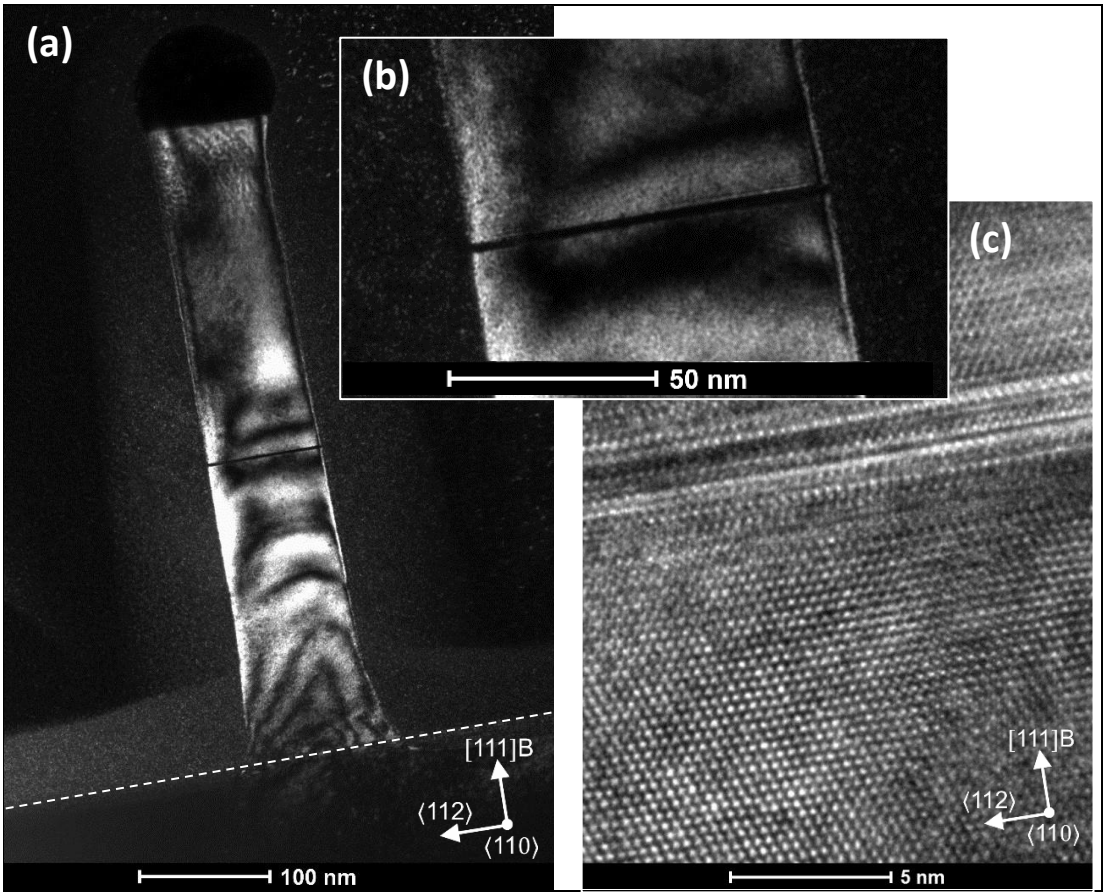

Figure S9: TEM investigation of a vertical nanowire (NW). The NW exhibits a number of stacking faults visible in the high resolution TEM image (a) and (c), as well as in the dark field micrograph (b).

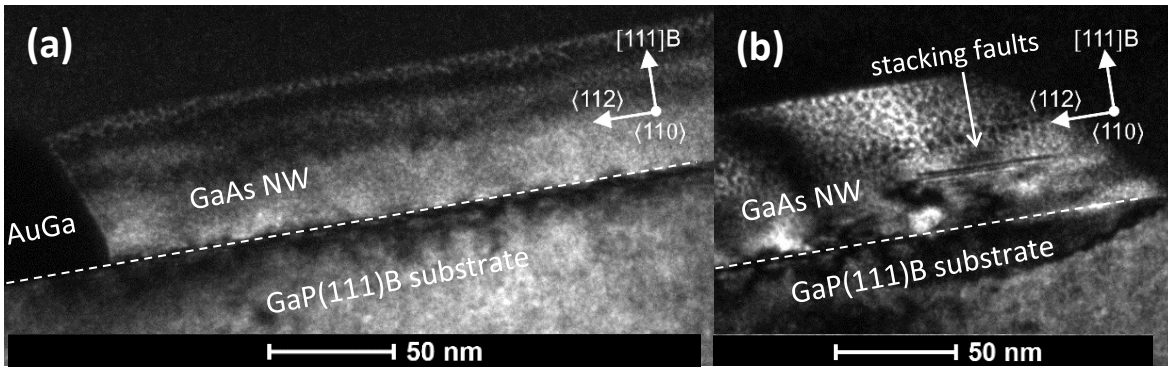

Figure S10: Darkfield TEM investigation of a horizontal GaAs nanowire (NW). The only visible defects are stacking faults (SF) in the region where NW growth initiates (b). These SFs are parallel to the substrate surface and correspond to nuclei on position (2) or (2') in the model. The NW is completely free of SFs (and other defects) parallel to its later growth front. Hence in full agreement with our growth model, no SFs are induced by nucleation at position (1').

S7 Numerical values for model parameters

The values for interface energies depend on the composition of the liquid AuGa (L) particle. For the AuGa particle of the horizontal NW, quantification of EDX spectra measured during TEM investigation yields 35% Ga. To account for Ga precipitation during cooldown after the growth process, we take $Ga_{0.4}Au_{0.6}$ as a reasonable estimate.[10] In the following the derivation of the interfacial energies for the heteroepitaxial NW growth is described (W = GaAs). For the liquid/GaAs interface we found $\gamma_{WL}^{(0.2)} = 6.24\,\frac{eV}{nm^2}$ and $\gamma_{WL}^{(1.0)} = 0.77\,\frac{eV}{nm^2}$ for a $Ga_{0.2}Au_{0.8}$ alloy and for pure Ga, respectively.[8,11] We interpolated these values linearly to $\gamma_{WL} = 4.87\,\frac{eV}{nm^2}$ for our expected Ga concentration of $Ga_{0.4}Au_{0.6}$. Likewise, energies for the liquid/vapor interface have been determined experimentally as $\gamma_{LV}^{(0.0)} \approx 7.45\,\frac{eV}{nm^2}$ and $\gamma_{LV}^{(1.0)} = 4.50\,\frac{eV}{nm^2}$.[12,13] Linear interpolation yields $\gamma_{LV} = 6.27\,\frac{eV}{nm^2}$. Due to the chemical similarity of GaAs and GaP, we assume that both have similar interface energies to the liquid gold $\gamma_{SL} \approx \gamma_{WL}$, which is also supported by experiment: if the values were dramatically different it would be impossible to grow straight NWs with both GaP on top of GaAs and GaAs on top of GaP.[14] There are slightly different values for the V-W interface in literature, with $5.12\,\frac{eV}{nm^2}$ for the $[111]_A$ polar and $4.31\,\frac{eV}{nm^2}$ for the $[111]_B$ polar interfaces, which are Ga- and P-terminated, respectively.[15] For our purposes, we take the average of those two values: $\gamma_{WV} = 4.72\,\frac{eV}{nm^2}$.

We did not find any experimental values for the interface energies of GaP/GaAs (*i.e.* the S-W interface). Therefore, we performed DFT slab calculations using the PBEsol functional (which is optimized for solids). In particular, we employed the Vienna Ab initio Simulation Package (VASP) code[16,17] and the projected-augmented-wave (PAW) approach[18] to represent the electron-ion interaction. Slabs in [111] direction with three, six and twelve layers were used, all agreeing on the same interface energies. We used a 19x19x3 k-grid and a kinetic energy cutoff at 500 eV. The S-W interface energy depends on the actual lattice constant a near the interface. It can be split into two contributions stemming from chemical interaction and elastic deformation, $\gamma_{SW}(a) = \gamma_{SW}^{\mathrm{chem}}(a) + \gamma_{SW}^{\mathrm{deform}}(a)$. In our simulation, $\gamma_{SW}^{\mathrm{deform}}$ and γ_{SW} between GaAs (W) and GaP (S) are obtained from a deformed slab. Necessarily, both materials are forced to have the same lateral lattice constant a (within the (111) plane), but are allowed to expand or contract freely in the [111] direction. First, we calculate the energy of deformed GaAs per mono-layer, $\varepsilon_{\mathrm{GaAs}}(a)$, by dividing the total energy from a DFT calculation by the number of applied monolayers, $\mathrm{N_{GaAs}}$. Second, we do the same for GaP. This allows us to calculate the strain-energy per monolayer, depending on the lattice constant a. Third, we perform a calculation with the III-V compounds GaAs and GaP periodically stacked on top of each other. From the total energy of this system $\mathrm{E_{tot}}(a) = \mathrm{N_{GaAs}}\varepsilon_{\mathrm{GaAs}}(a) + \mathrm{N_{GaP}}\varepsilon_{\mathrm{GaP}}(a) + \Delta\mathrm{E_{chem}}(a)$ we can calculate (by subtraction) the chemical contribution to the interface energy. This energy contains contributions from both the GaAs/GaP and GaP/GaAs interface. Thus, dividing $\Delta\mathrm{E_{chem}}(a)$ by twice the interface area, $\mathrm{A}(a)$, we obtain an average of $\Delta\gamma_{SW}^{\mathrm{chem}}(a)$. For an average lattice constant near the interface this results in $\Delta\gamma_{SW}(a) = 0.77\,\frac{eV}{nm^2}$ with $\Delta\gamma_{SW}^{\mathrm{chem}}(a) = 0.00\,\frac{eV}{nm^2}$ (numerically zero within the two-digit accuracy). If the GaP substrate is

kept rigid and an additional monolayer of GaAs is forced to the GaP lattice constant, DFT calculations show that this requires $\Delta\gamma_{SW}(a_{\mathrm{GaP}}) = 1.49\,\frac{eV}{nm^2}$ with $\Delta\gamma_{SW}^{\mathrm{chem}}(a_{\mathrm{GaP}}) = 0.12\,\frac{eV}{nm^2}$. Thus, γ_{SW} is clearly dominated by the deformation energy $\gamma_{SW}^{\mathrm{deform}}$ and the chemical interaction is comparably small or even negligible (as it might be expected for a material that is known to form GaAsP alloys[19]). In reality, the lattice parameter a will vary with height such that the deformation stress is maximal near the interface plane and quickly decays away from it – which might result in a slightly different value for the effective $\Delta\gamma_{SW}(a)$. Still, the conclusions of our model are unaffected by such small changes, as shown in the next section.

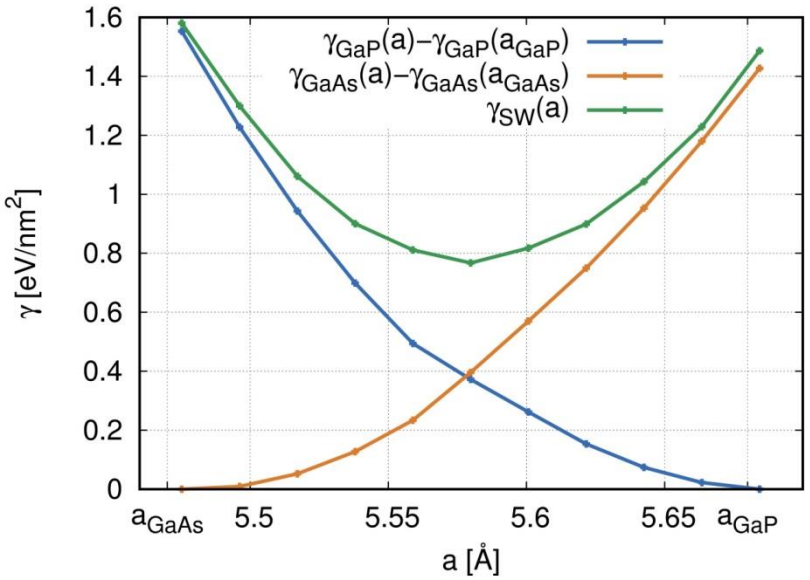

Figure S11: Interface energy γ depending on the lattice constant a for an GaP(111) / GaAs(111) interface based on our DFT calculations. The blue (orange) line shows the deformation energy per monolayer needed for GaP (GaAs). The green line represents results from a calculation with a deformed slab containing both materials. Since the green line is almost equal to the sum of the blue and orange one, we conclude that the interface energy is dominated by deformation.

S8 Sensitivity on model parameters

Our model for homo- and hetero-nucleation probabilities involves interface energies and geometry factors. Since some of the parameters were obtained by interpolation or reasonable assumptions, we discuss in this section the sensitivity of our predictions with respect to the choice of parameters. We start with the geometry parameters: Any shape of the nucleus with aspect ratios b/c similar to that of a hexagon (take as a fictitious example, a circle with $b = c = 2\pi$) results in very similar results for $p_i(\Delta\mu)$. As an example for a different possible nucleus shape, we consider the equilateral triangle. In this case, $b = 3\sqrt{3}$, $c = b/2$ and twice of the lateral nucleus area is in contact with other materials, *i.e.* all $\alpha = \beta = \vartheta = 1/3$ (instead of $1/6$). The resulting nucleation probabilities are plotted in Figure S12a. Clearly, the same nucleation positions are dominant, even though minor quantitative differences exist. We conclude that different geometrical shapes do not change the predictions of our model in any qualitative way.

Further, we study the sensitivity of our model with respect to the choice of interface energies. In particular, we consider for γ_{WV} the values between which we interpolated. For γ_{LV} and γ_{WL} we use the values for $Ga_{0.2}Au_{0.8}$ and $Ga_{0.5}Au_{0.5}$ and for γ_{SW} we use significantly lower values than obtained from our DFT calculations to underline the robustness of the model. The results are plotted in Figure S12b and it is again obvious that our predictions are qualitatively unaffected.

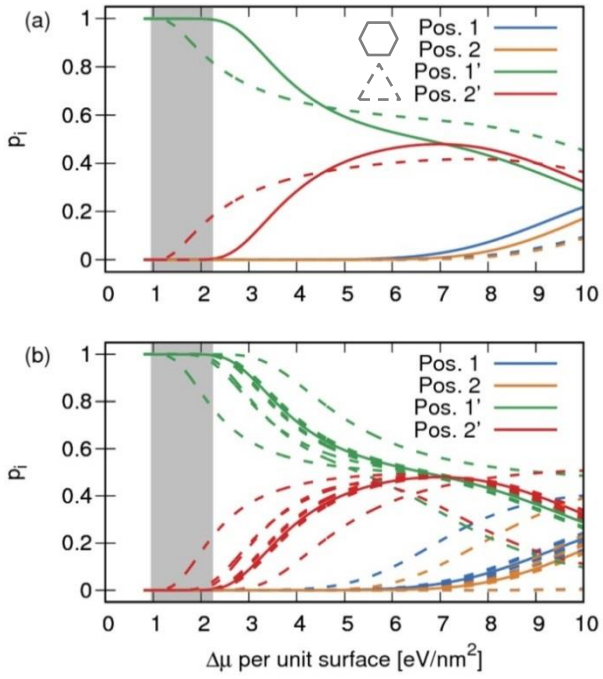

Figure S12: Nucleation probabilities p_i for the different positions discussed in the main text. The solid lines correspond to the parameters chosen in Figure 6 of the main text. If the nucleus is assumed to be an equilateral triangle, the dashed curves in (a) are obtained. In (b) we plot p_i for three sets of different numerical values for the interface energies (*ceteris paribus* as dashed lines: γ_{WV} = 4.31 or 5.12 eV/nm², γ_{LV} = 5.98 or 6.86 eV/nm², $\gamma_{WL} = \gamma_{SL}$ = 4.19 or 6.24 eV/nm²) and γ_{SW} = 0.25 or 0.54 eV/nm²), which differ considerably from those used in Figure 6 of the main text. The probabilities depend on the chemical potential per unit area ($\varrho h \Delta\mu$), where the range relevant to experiment is highlighted in gray.

S9 GaAsP nanowires and other hetero-systems

In addition, we studied further III-V-hetero-systems, both theoretically and experimentally. For the ternary system of $GaAs_{1-x}P_x$-NWs on GaP(111)B, we linearly interpolated the interface energies of the participating interfaces for growth of pure GaP- and GaAs-NWs on GaP(111)B. While γ_{SL}, γ_{WL} and γ_{LV} are independent of the P-ratio x, some interface energies vary with increasing x: $\gamma_{WV} = 4.72 \ldots 10.5 \frac{eV}{nm^2}$ (Refs. 15,20) and $\gamma_{SW} = 0.77 \ldots 0 \frac{eV}{nm^2}$ (*cf.* section S7). For the same parameters as chosen for Figure 6 (compare section S7) this yields the nucleation probabilities shown in Figure 8. Experimental data, confirming the theoretical predictions, are shown in Figure S13.

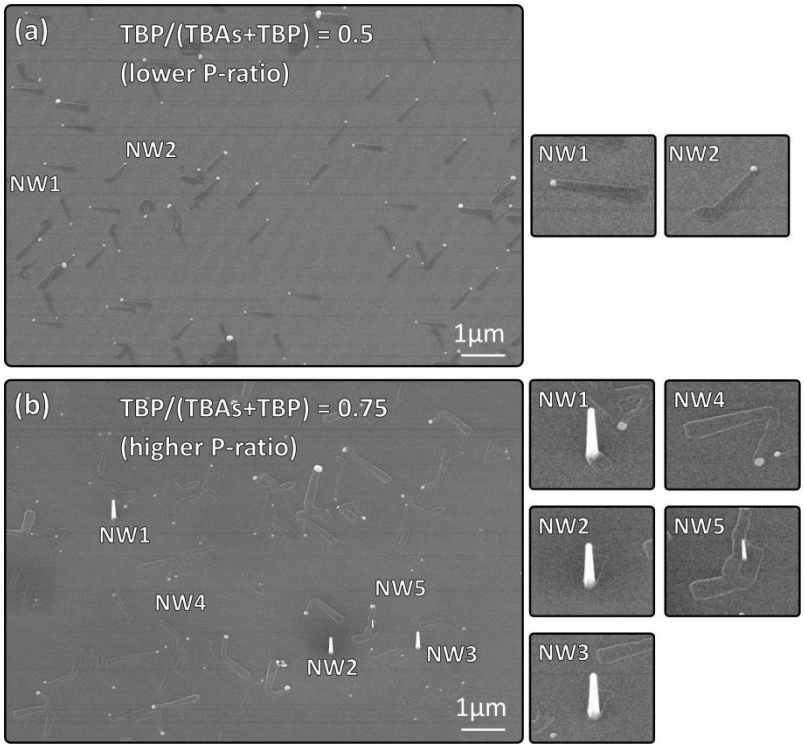

Figure S13: GaAsP nanowires grown on GaP(111)B with different ratios between the P- and the As-precursor (TBP and TBAs, respectively). For both samples V/III was 20 and the growth temperature was 475°C. In both cases nucleation conditions led exclusively to growth of NWs, which are initially horizontal. While for the lower P-ratio (a), *i.e.* relatively high lattice mismatch, all NWs remain horizontal, some of the NWs change from horizontal to vertical growth for the higher P-ratio (b) as it is predicted by the calculations shown in Figure 8. Note the different contrast between NWs and substrate for (a) and (b) due to different material compositions.

For the other hetero-systems presented in Figure S14, we obtained the interface energies between two III/V materials, A and B, from DFT calculations in analogy to GaAs/GaP, which is presented in section S7. For an average lattice constant near the interface this results in the values listed in Table S1. For the other interface energies we found values in the literature. For a high comparability, we chose the values for γ_{WV} from the same source as for GaP-NWs (Ref. 20): 5.36 $\frac{eV}{nm^2}$ InAs-NWs and 6.98 $\frac{eV}{nm^2}$ for InP-NWs. Values for γ_{WL} were chosen as in Refs. 21 and 22, with 3.6 $\frac{eV}{nm^2}$ for InAs-NWs and 5.0 $\frac{eV}{nm^2}$ for InP-NWs, which they estimated assuming $\gamma_{WL} \approx \gamma_{WV}$. In accordance to section S7, we took $\gamma_{WL} = 4.87 \frac{eV}{nm^2}$ both for GaAs- and GaP-substrates, neglecting that dissolution of In instead of Ga during InAs- or InP-NW growth will

slightly change this value. For both InAs- and InP-NWs, we chose $\gamma_{LV} = 5.6\,\frac{eV}{nm^2}$ according to Ref. 22, which lies between the values for liquid Au and In.

Table S1: 111-interface energies in eV/nm² determined by DFT slab calculations used for Figure S13. γ_{SW} comprises a deformation contribution by strain and a chemical contribution.

	γ_{SW}	$\gamma_{SW}^{\mathrm{deform}}$	$\gamma_{SW}^{\mathrm{chem}}$
GaP / InP	3.19	3.10	0.09
GaAs / InAs	2.48	2.36	0.12
GaAs / InP	1.29	0.44	0.85

Figure S14 shows that our model predicts nucleation at position (1') and, hence, elongated horizontal growth in a wide range of $\Delta\mu$ for all studied systems. The widest range in $\Delta\mu$ for nucleation at Position (1') is present for InP-NWs on GaP(111)B. This is mostly due to the high value of γ_{SW}. Although for InAs-NWs on GaAs(111)B the value of γ_{SW} is only a little less (compared to InP on GaP), the nucleation probability at (1') decreases at comparably low $\Delta\mu$. This is because of $\gamma_{WL} < \gamma_{SL}$, which leads to rather small $\Delta\gamma$ and thereby favors position (2'). Despite the comparable lattice mismatch for the systems GaP/GaAs ($\Delta a = 3.7\%$) and GaAs/InP ($\Delta a = 3.8\%$), the nucleation probability at (1') drops at lower $\Delta\mu$ values in case of GaAs/InP. This is due to the rather great chemical dissimilarity, which leads to significant chemical contributions to γ_{SW}.

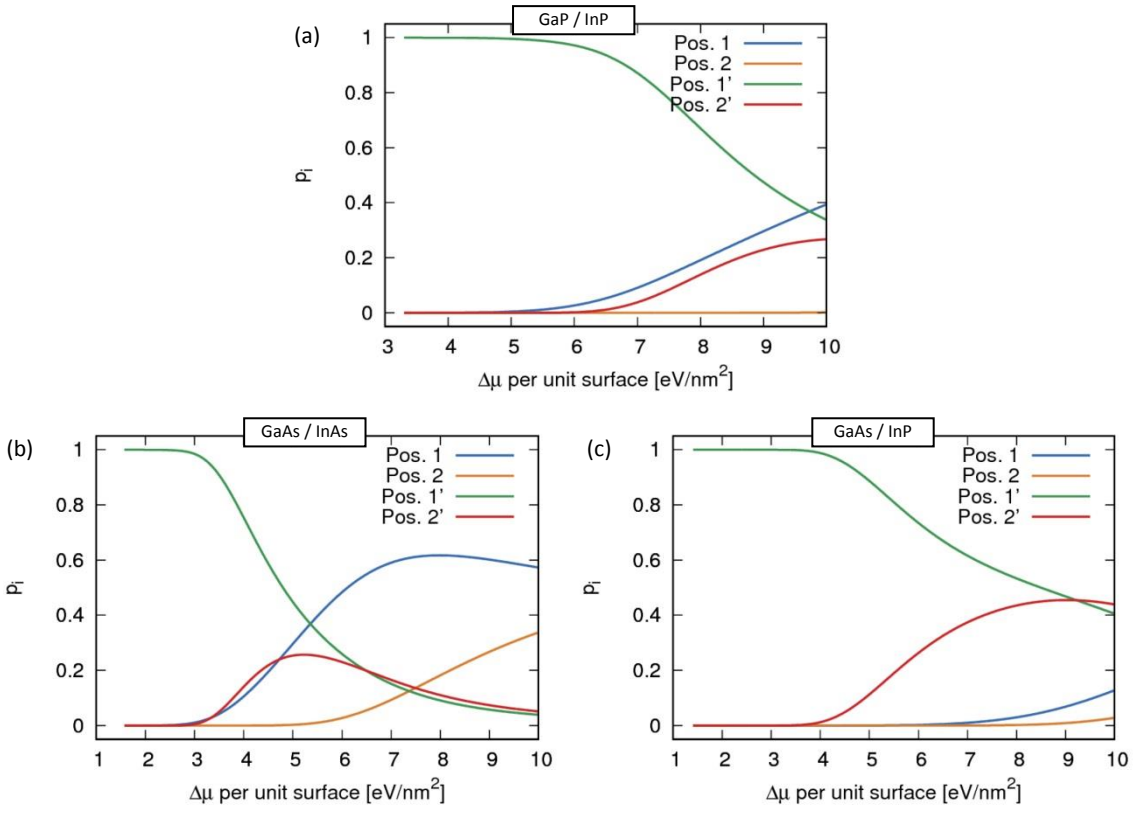

Figure S14: Nucleation probabilities p_i for different hetero-systems assuming hexagonal nuclei with $\alpha = \beta = \vartheta = 1/6$. (a) InP-NWs on GaP(111)B, (b) InAs-NWs on GaAs(111)B and (c) InP-NWs on GaAs(111)B. Note that the curves are only drawn for $\Delta\mu$, at which nucleation can happen. This range can be obtained from equation (5) by requiring the critical nucleation radius to be positive, *i.e.* $\rho h\Delta\mu > \Delta\gamma$.

References

(1) Uccelli, E.; Arbiol, J.; Magen, C.; Krogstrup, P.; Russo-Averchi, E.; Heiss, M.; Mugny, G.; Morier-Genoud, F.; Nygård, J.; Morante, J. R.; *et al.* Three-Dimensional Multiple-Order Twinning of Self-Catalyzed GaAs Nanowires on Si Substrates. *Nano Lett.* **2011**, *11*, 3827–3832.

(2) Fortuna, S. A.; Li, X. Metal-Catalyzed Semiconductor Nanowires: A Review on the Control of Growth Directions. *Semicond. Sci. Technol.* **2010**, *25*, 24005.

(3) Fonseka, H. A.; Caroff, P.; Wong-Leung, J.; Ameruddin, A. S.; Tan, H. H.; Jagadish, C. Nanowires Grown on InP (100): Growth Directions, Facets, Crystal Structures, and Relative Yield Control. *ACS Nano* **2014**, *8*, 6945–6954.

(4) Bakkers, E.; Borgstrom, M.; Verheijen, M. Epitaxial Growth of III-V Nanowires on Group IV Substrates. *MRS Proc.* **2008**, *1068*, 1068-C02-4.

(5) Krishnamachari, U.; Borgstrom, M.; Ohlsson, B. J.; Panev, N.; Samuelson, L.; Seifert, W.; Larsson, M. W.; Wallenberg, L. R. Defect-Free InP Nanowires Grown in [001] Direction on InP (001). *Appl. Phys. Lett.* **2004**, *85*, 2077.

(6) Schwarz, K. W.; Tersoff, J. From Droplets to Nanowires: Dynamics of Vapor-Liquid-Solid Growth. *Phys. Rev. Lett.* **2009**, *102*, 1–4.

(7) Schwarz, K. W.; Tersoff, J. Multiplicity of Steady Modes of Nanowire Growth. *Nano Lett.* **2012**, *12*, 1329–1332.

(8) Glas, F.; Harmand, J.-C.; Patriarche, G. Why Does Wurtzite Form in Nanowires of III-V Zinc Blende Semiconductors? *Phys. Rev. Lett.* **2007**, *99*, 146101.

(9) Dubrovskii, V. G. *Nucleation Theory and Growth of Nanostructures*; Springer: Saint Petersburg, 2014.

(10) Harmand, J. C.; Patriarche, G.; Péré-Laperne, N.; Merat-Combes, M. N.; Travers, L.; Glas, F. Analysis of Vapor-Liquid-Solid Mechanism in Au-Assisted GaAs Nanowire Growth. *Appl. Phys. Lett.* **2005**, *87*, 1–3.

(11) Glas, F.; Ramdani, M. R.; Patriarche, G.; Harmand, J.-C. Predictive Modeling of Self-Catalyzed III-V Nanowire Growth. *Phys. Rev. B* **2013**, *88*, 195304.

(12) Jasper, J. J. The Surface Tension of Pure Liquid Compounds. *J. Phys. Chem. Ref. Data* **1972**, *1*, 841.

(13) Zangwill, A. *Physics at Surfaces*; Cambridge University Press: Cambridge, 1988.

(14) Dick, K. A.; Kodambaka, S.; Reuter, M. C.; Deppert, K.; Samuelson, L.; Seifert, W.; Wallenberg, L. R.; Ross, F. M. The Morphology of Axial and Branched Nanowire Heterostructures. *Nano Lett.* **2007**, *7*, 1817–1822.

(15) Moll, N.; Kley, A.; Pehlke, E.; Scheffler, M. GaAs Equilibrium Crystal Shape from First Principles. *Phys. Rev. B* **1996**, *54*, 8844–8855.

(16) Kresse, G.; Hafner, J. Ab Initio Molecular Dynamics for Liquid Metals. *Phys. Rev. B* **1993**, *47*, 558–561.

(17) Kresse, G.; Furthmüller, J. Efficient Iterative Schemes for Ab Initio Total-Energy Calculations Using a Plane-Wave Basis Set. *Phys. Rev. B* **1996**, *54*, 11169–11186.

(18) Blöchl, P. E. Projector Augmented-Wave Method. *Phys. Rev. B* **1994**, *50*, 17953–17979.

(19) Adachi, S. Properties of Semiconductor Alloys: Group-IV, III-V and II-VI Semiconductors. In; John Wiley & Sons, 2009; p. 175.

(20) Sibirev, N. V; Timofeeva, M. A.; Bol'shakov, A. D.; Nazarenko, M. V; Dubrovskiĭ, V. G. Surface Energy and Crystal Structure of Nanowhiskers of III–V Semiconductor Compounds. *Phys. Solid State* **2010**, *52*, 1531–1538.

(21) Algra, R. E.; Verheijen, M. a; Borgström, M. T.; Feiner, L.-F.; Immink, G.; van Enckevort, W. J. P.; Vlieg, E.; Bakkers, E. P. a M. Twinning Superlattices in Indium Phosphide Nanowires. *Nature* **2008**, *456*, 369–372.

(22) Joyce, H. J.; Wong-Leung, J.; Gao, Q.; Tan, H. H.; Jagadish, C. Phase Perfection in Zinc Blende and Wurtzite III−V Nanowires Using Basic Growth Parameters. *Nano Lett.* **2010**, *10*, 908–915.